

LETTER TO THE EDITOR

Implications of multiwavelength spectrum on cosmic-ray acceleration in blazar TXS 0506+056

Saikat Das¹, Nayantara Gupta², and Soebur Razzaque^{3,4,5}

¹ Center for Gravitational Physics, Yukawa Institute for Theoretical Physics, Kyoto University, Kyoto 606-8502, Japan
e-mail: saikat.das@yukawa.kyoto-u.ac.jp

² Astronomy & Astrophysics Group, Raman Research Institute, Bangalore 560080, Karnataka, India
e-mail: nayan@rri.res.in

³ Centre for Astro-Particle Physics (CAPP) and Department of Physics, University of Johannesburg, PO Box 524, Auckland Park 2006, South Africa
e-mail: srizzaque@uj.ac.za

⁴ Department of Physics, The George Washington University, Washington, DC 20052, USA

⁵ National Institute for Theoretical and Computational Sciences (NITheCS), South Africa

Received YYYY; accepted ZZZZ

ABSTRACT

Context. The MAGIC collaboration has recently analyzed data from a long-term multiwavelength campaign of the γ -ray blazar TXS 0506+056. In December 2018, it was flaring in the very-high-energy (VHE; $E > 100$ GeV) γ -ray band, but no simultaneous neutrino event was detected.

Aims. We explore prospects for detecting γ -rays and neutrinos of hadronic origin, produced both inside and outside the jet of TXS 0506+056, while coherently modeling the observed spectral energy distribution (SED) and neutrino flux upper limits.

Methods. We constrain the neutrino flux through the restriction from observed X-ray flux on the secondary radiation due to hadronic cascade. We propagate the escaping ultra-high-energy cosmic rays (UHECRs; $E \gtrsim 0.1$ EeV) in a random, turbulent extragalactic magnetic field (EGMF).

Results. The leptonic emission from the jet dominates the GeV range, whereas the cascade emission from CR interactions in the jet contributes substantially to the X-ray and VHE range. The line-of-sight cosmogenic γ rays from UHECRs produce a hardening in the VHE range of the SED. Neutrino signal from the jet showed little or no variability during the MAGIC campaign. Therefore, we infer that the correlation between VHE γ -rays and neutrino flare is minimal. The luminosity in CRs limits the cosmogenic γ -ray flux, which, in turn, bounds the RMS value of the EGMF to $\gtrsim 10^{-5}$ nG. The cosmogenic neutrino flux is lower than the IceCube-Gen2 detection potential for 10 yrs of observation.

Conclusions. VHE γ -ray variability should arise from an increased activity inside the jet. Upcoming γ -ray imaging telescopes, such as the CTA, will be able to constrain the cosmogenic γ -ray component in the SED of TXS 0506+056. Detecting a steady flux at multi-TeV energies will validate blazars as unambiguous sources of UHECRs.

Key words. Astroparticle physics – galaxies: active – gamma-rays: general – neutrinos

1. Introduction

Blazars are a subclass of radio-loud Active Galactic Nuclei (AGNs), with their highly relativistic jet collimated towards the observer's line of sight. They have been considered as prominent candidates for the origin of IceCube-detected diffuse astrophysical neutrino flux beyond ~ 10 TeV (IceCube Collaboration et al. 2013; Eichler 1979; Sikora et al. 1987; Petropoulou et al. 2015; Yuan et al. 2020) and may also contribute in the PeV-EeV energy range (Kalashev et al. 2013; Kochocki et al. 2021; Das et al. 2021). For the first time in September 2017, a high-energy muon-neutrino event IC-170922A ($E_\nu \sim 0.3$ PeV) was associated with the γ -ray flaring blazar TXS 0506+056 at 3σ significance (Aartsen et al. 2018a). Subsequently, other events having positional coincidence with Fermi-LAT detected blazars are also observed with lower statistical significance (Garrappa et al. 2019; Franckowiak et al. 2020). Despite several studies on this object, it is crucial to revisit the spectral properties for predicting the multi-messenger signals from similar sources.

The explanation of the neutrino event requires synchrotron (SYN) and synchrotron self-Compton (SSC) photons as the target for $p\gamma$ interactions (Cerruti et al. 2019). Whereas, other models require an external photon field, resulting in external inverse-Compton (IC) emission (Reimer et al. 2019; Keivani et al. 2018; Petropoulou et al. 2020). In the hadronuclear interpretation via pp interaction, the shock accelerated protons may interact with gas clouds in the vicinity of the supermassive black hole (Liu et al. 2019) or cold protons in the jet (Banik & Bhadra 2019). Some studies invoke neutrino production from the interaction of relativistic neutron beams in the jet, originating in $p\gamma$ interactions with external photons (Zhang et al. 2020).

The CR-induced cascade from Bethe-Heitler (BH) pair production contributes near the X-ray energies in the $p\gamma$ scenario, thus also limiting the hadronic component in GeV-TeV γ -rays. As a result, this constrains the astrophysical neutrinos, in many cases, to a flux level lower than predicted by IceCube observations. Thus, an additional photon field of energy $\epsilon \approx m_\pi m_p c^4 / 20 E_\nu \approx 440$ eV, i.e., in the UV to soft X-ray energy

band, is required. However, an ‘‘orphan’’ neutrino flare from this source from September 2014 to March 2015 is revealed from the analysis of archival data, at 3.5σ statistical significance (Aartsen et al. 2018b). The latter was not accompanied by increased activity in γ -rays, indicating a different mechanism for neutrino and γ -ray flares. Often, a two-zone model is employed, considering a high opacity for GeV γ -rays in the neutrino production region (Sahakyan 2018; Xue et al. 2021).

Recently, the MAGIC collaboration has modeled the spectrum of TXS 0506+056, observed during a multiwavelength campaign lasting 16 months from November 2017 to February 2019, covering the radio band, optical/UV, high-energy, and very-high-energy (VHE, $E > 100$ GeV) γ -rays (Acciari et al. 2022). A flaring activity was observed by MAGIC during December 2018. Fermi-LAT observed several short flares on timescales of days to weeks, unlike the long-term flare of 2017. At lower energies, no significant variability was observed. The observed flare was not associated with any neutrino event. Their model infers the neutrino luminosity to be lower than the detection threshold of currently operating instruments.

We analyze the multiwavelength SED using a one-zone leptohadronic model. The low-energy peak results from the SYN radiation of relativistic electrons. The high-energy peak is produced by SSC and IC scattering of external photons (external Compton, *abbr.* EC). These external photons may originate from the broad-line region (BLR). Although a broad-line emission in the optical spectrum is not detected, TXS 0506+056 can be a masquerading BL Lac, *i.e.*, intrinsically a flat spectrum radio quasar (FSRQ) with hidden broad lines and a standard accretion disk (Padovani et al. 2019). The interaction of the cosmic ray protons with the leptonic radiation and the external photon field produces a characteristic photon spectrum resulting from the electromagnetic cascade of secondary electrons, which is constrained by the X-ray data.

Blazars are also suitable candidates for ultrahigh-energy cosmic ray (UHECR; $E \gtrsim 10^{18}$ eV) acceleration. They can escape the jet and interact with cosmic background photons. In an earlier work, the neutrino flux originating in extragalactic propagation of UHECRs from TXS 0506+056, and a few other blazars was analyzed (Das et al. 2022). We assumed a correlation between the cosmic-ray and IceCube-detected neutrino luminosity inside the jet, to scale the cosmogenic fluxes. Here, we constrain the UHECR luminosity by SED modeling, consistently with the allowed flux of cosmogenic γ -rays. The EGMF is crucial to determine the line-of-sight resolved component. Using the latest spectrum data, we coherently explain the multiwavelength SED, the neutrino flux from the jet emission region, and the plausibility of cosmogenic γ -ray contribution to the SED. Finally, the luminosity constraint can be used to predict the resulting cosmogenic neutrino flux at EeV energies.

2. Results

2.1. Radiative Modeling

We consider the emission region in the jet to be a spherical blob of radius R' , consisting of a relativistic plasma of electrons and protons moving through a uniform magnetic field B . The bulk Lorentz factor of the jet is Γ and the doppler factor is given by $\delta_D = [\Gamma(1 - \beta \cos \theta)]^{-1}$, where βc is the velocity of the emitting plasma and θ is the viewing angle. For $\theta \lesssim 1/\Gamma$, $\Gamma \approx \delta_D$. We inject electrons in the blob with a spectrum

$$Q'_e(\gamma'_e) = A_e(\gamma'_e/\gamma_0)^{-\alpha-\beta \log_{10}(\gamma'_e/\gamma_0)} \quad \text{for } \gamma'_{e,\min} < \gamma'_e < \gamma'_{e,\max} \quad (1)$$

to fit the observed broadband SED. The normalization of the spectrum A_e depends on the luminosity of injected electrons, and $\gamma_0 m_e c^2$ is a reference energy fixed at 500 MeV. A quasi-steady state is reached when the injection is balanced by radiative cooling and/or escape. Empirically, the steady state electron density distribution is given as $N'_e(\gamma'_e) = Q'_e(\gamma'_e)t'_e$, where $t'_e = \min\{t'_{\text{cool}}, t'_{\text{esc}}\}$. We consider the escape timescale $t'_{\text{esc}} \approx t'_{\text{dyn}} = 2R'/c$. The radiative cooling timescale is given as

$$t'_{\text{cool}} = \frac{3m_e c}{4(u'_B + \kappa_{\text{KN}} u'_{\text{ph}}) \sigma_T \gamma'_e} \quad (2)$$

Here $u'_B = B^2/8\pi$ is the energy density in magnetic field, u'_{ph} is the energy density of soft photons, σ_T is the Thomson scattering cross-section, and κ_{KN} accounts for the suppression of IC emission due to the Klein-Nishina effect. We use the open-source code GAMERA to solve the transport equation for obtaining the injection spectrum at time t' (Hahn 2016),

$$\frac{\partial N'_e}{\partial t} = Q'_e(\gamma'_e, t') - \frac{\partial}{\partial \gamma'_e} (b N'_e) - \frac{N'_e}{t'_{\text{esc}}} \quad (3)$$

where $b = b(\gamma'_e, t')$ is the energy loss rate of electrons.

The steady-state electron spectrum yields the SYN and SSC emission. In addition, we consider an external photon field, which is Compton upscattered by the same electrons. It is considered to be a blackbody with temperature (T') and energy density $u'_{\text{ext}} = (4/3)\Gamma^2 u_{\text{ext}}$ in the jet frame, where the energy density in the AGN frame is $u_{\text{ext}} = \eta_{\text{ext}} L_{\text{disk}}/4\pi R_{\text{ext}}^2 c$ and η_{ext} is the fraction of the disk luminosity.

The proton injection spectrum is given by a power-law $Q'_p(\gamma'_p) = A_p \gamma'^{-\alpha}$. The steady-state proton spectrum is then given as $N'_p(\gamma'_p) = Q'_p(\gamma'_p)t'_p$, where $t'_p = \min\{t'_{p\gamma}, t'_{\text{BH}}, t'_{p,\text{syn}}, t'_{\text{esc}}\}$. The escape timescale is the same as that for electrons. The main energy loss processes of the protons are pion production ($p\gamma \rightarrow p + \pi^0$ or $n + \pi^+$) and BH process ($p\gamma \rightarrow p + e^+e^-$). The seed photons are the leptonic emission and external photons. The charged pions decay to produce neutrinos. The timescale of these interactions can be expressed as follows

$$\frac{1}{t'_{p\gamma}} = \frac{c}{2\gamma_p'^2} \int_{\epsilon_{\text{th}}/2\gamma_p}^{\infty} d\epsilon'_\gamma \frac{n(\epsilon'_\gamma)}{\epsilon_\gamma'^2} \int_{\epsilon_{\text{th}}}^{2\epsilon\gamma_p} d\epsilon_r \sigma(\epsilon_r) K(\epsilon_r) \epsilon_r \quad (4)$$

where $\sigma(\epsilon_r)$ and $K(\epsilon_r)$ are the cross-section and inelasticity respectively of photopion production or BH pair production as a function of photon energy ϵ_r in the proton rest frame. $n(\epsilon'_\gamma)$ is the target photon number density (Stecker 1968).

The spectrum of γ rays from the decay of neutral pions and the spectrum of e^+e^- due to BH process are calculated using the parametrization by Kelner & Aharonian (2008). The proton injection is weighed by the corresponding rates $R_{p\gamma/\text{BH}}/R_{\text{tot}}$, where $R_{\text{tot}} = R_{p\gamma} + R_{\text{BH}}$. The high-energy γ rays are absorbed by $\gamma\gamma \rightarrow e^\pm$ pair production with the leptonic emission, leading to attenuation of TeV γ -rays. The escaping γ -ray flux is given as

$$Q'_{\gamma,\text{esc}}(\epsilon'_\gamma) = Q'_{\gamma,\pi}(\epsilon'_\gamma) \left(\frac{1 - \exp(-\tau_{\gamma\gamma})}{\tau_{\gamma\gamma}} \right) \quad (5)$$

We calculate $\tau_{\gamma\gamma}$ using the formalism given by Gould & Schröder (1967) to calculate the absorption probability per unit path length for an isotropic photon field,

$$I_{\gamma\gamma}^{-1}(\epsilon'_\gamma) = \frac{1}{2} \int \int n(\epsilon'_k) \sigma_{\gamma\gamma}(\epsilon'_\gamma, \epsilon'_k, \theta) (1 - \cos \theta) \sin \theta d\theta d\epsilon'_k \quad (6)$$

where $\sigma_{\gamma\gamma}$ is the full pair-production cross-section and the $n(\epsilon'_k)$ is the combined density of soft photons and external radiation.

The high-energy electrons and positrons produced in $\gamma\gamma$ pair production ($Q'_{e,\gamma\gamma}$), charged pion decay ($Q'_{e,\pi}$), and BH process ($Q'_{e,BH}$) can initiate cascade radiation from the jet. We solve the steady state spectrum of secondary electrons ($N'_{e,s}(\gamma_e)$) in the jet frame using the analytical approach of Boettcher et al. (2013), including $Q'_{e,BH}$ in the source term. In a synchrotron-dominated cascade, emission from secondary electrons is given by

$$Q'_s(\epsilon'_s) = A_0 \epsilon'^{-3/2} \int_1^\infty d\gamma'_e N'_{e,s}(\gamma'_e) \gamma_e'^{-2/3} e^{-\epsilon'_s/b\gamma_e'^2} \quad (7)$$

with $A_0 = c\sigma_T B'^2/[6\pi m_e c^2 \Gamma(4/3)b^{4/3}]$ being a normalization constant, where $b = B'/B_{\text{crit}}$ and $B_{\text{crit}} = 4.4 \times 10^{13}$ G.

2.2. Multiwavelength SED

During the multiwavelength campaign, the source was monitored using the Swift-XRT, Swift-UVOT, and NuSTAR, maximizing the simultaneity of observation with the MAGIC telescope (Acciari et al. 2022). From November 2017 to February 2019, a total of ~ 79 hrs of good-quality data was collected by MAGIC. During most of this period (~ 74 hrs), the source was found to be in a low-state with average photon flux $F(> 90 \text{ GeV}) = (2.7 \pm 2.1) \times 10^{-11} \text{ erg cm}^{-2} \text{ s}^{-1}$. Fermi-LAT data was also used in the spectral analysis. For the flaring state of December 2018, only simultaneous data is obtained by Fermi-LAT and MAGIC in the GeV and VHE γ -rays, and by ASAS-SN in the optical. The integral photon flux observed by MAGIC rose by an order of magnitude compared to the low state. The most significant variability was observed in the GeV band, while the X-ray variability was found to be at a lower level. The radio, optical and UV bands showed moderate variability (Acciari et al. 2022).

The γ -ray variability timescale of TXS 0506+056 observed in October 2017 was shown to be $t_{\text{var}} \leq 10^5$ s (Keivani et al. 2018). The γ -ray flare of December 2018 was found to be very similar. The size of the emission region inferred from the variability is $R' \lesssim \delta_D c t_{\text{var}}/(1+z) \approx 6.75 \times 10^{16} (\delta_D/30)(t_{\text{var}}/10^5 \text{ s}) \text{ cm}$. We assume the radius of the emission region to be 10^{16} cm and $\Gamma \approx \delta_D$ during both the high- and low-states. The magnetic field is also assumed to be the same in the two states, $B' = 0.28$ G. The value is considered such that the muons and pions produced in hadronic interactions do not suffer significant energy losses before decaying.

The luminosity distance of TXS 0506+056 is $d_L \approx 1837$ Mpc, with a redshift of $z = 0.3365$. The total kinetic power in the jet is calculated as $L_{\text{kin}} = L_e + L_p + L_B = \pi R'^2 \Gamma^2 c (u'_e + u'_p + u'_B)$. The maximum electron energy changes from $\gamma'_{e,\text{max}} = 2 \times 10^4$ in the low-state to $\gamma'_{e,\text{max}} = 5 \times 10^4$ in the high-state to account for the spectral variability. We vary the maximum proton energy ($E'_{p,\text{max}}$) in the comoving jet frame over a wide range to find the best-fit value of 6.3 PeV, fixed for both the low- and high-states. The cascade emission from the steady-state secondary electron spectrum $N'_{e,s}$ is shown by the red lines in Fig. 1. The low energy peak of the cascade emission originates from the BH cascade, which is severely constrained by the X-ray data. As a result the pion decay cascade at higher energies is also limited and the contribution to the high-energy peak is not significant.

We obtain $T' = 2 \times 10^5$ K and $u'_{\text{ext}} = 0.01 \text{ erg/cm}^3$ for the external photon field from fitting the SED, which is the most important target of $p\gamma$ interaction for neutrino production and for IC scattering, crucial to explain the VHE spectrum. It is also vital for $\gamma\gamma$ absorption in the jet, beyond a few hundreds of GeV.

Table 1. Model parameters for the multiwavelength SED

Parameters	Low State	High State
δ_D	28	"
B' [G]	0.28	"
R' [cm]	10^{16}	"
u'_{BLR} [erg/cm ³]	0.01	"
T'_{BLR} [K]	2×10^5	"
α (e/p spectral index)	2.0	"
β (log parabola index)	0.3	"
E_0 [MeV]	500	"
$E'_{e,\text{min}}$ [GeV]	0.20	0.25
$E'_{e,\text{max}}$ [GeV]	10	25
L_e^{obs} [erg/s]	5.8×10^{44}	7.6×10^{44}
$E'_{p,\text{min}}$ [GeV]	10	"
$E'_{p,\text{max}}$ [PeV]	6.3	"
L_p^{obs} [erg/s]	1.6×10^{48}	"

For a typical disk luminosity $L_{\text{disk}} \approx 10^{46} \text{ erg/s}$ and the scattered disk emission to be a fraction $\eta_{\text{ext}} \sim 0.01$ of the disk photon energy density, R_{ext} comes out to be a few times 10^{18} cm .

The VHE flare of December 2018 does not have simultaneous observation at lower energies. Thus the constraints on the theoretical model is moderate. Nevertheless, to reduce the uncertainties, only the electron primary distribution and its corresponding luminosity is changed with respect to the low state. The parameter values used in the modeling are given in Tab. 1.

We fit the low-state spectrum first and optimize the parameters δ_D , B' , and spectral indices, using the leptonic emission only. The SYN spectrum peaks at optical band and a log-parabola injection spectrum of electrons well explains the data. The hadronic component is then added and the power and maximum proton energy is varied to fit the x-ray data with BH cascade. The VHE photon flux upper limits constrain the contribution from pion-decay cascade. We also consider absorption of VHE γ -rays in the extragalactic background light (EBL) using the Gilmore et al. model (Gilmore et al. 2012). The resulting muon neutrino flux from $p\gamma$ interactions is calculated as

$$E_\nu^2 J_\nu = \frac{1}{3} \frac{V' \delta_D^2 \Gamma^2}{4\pi d_L^2} E_\nu'^2 Q'_{\nu,p\gamma} \quad (8)$$

where the factor 1/3 corresponds to neutrino oscillation and $Q'_{\nu,p\gamma}$ is the total electron and muon neutrino flux from charged pion decay in the comoving frame. It can be seen from the left panel of Fig. 1, the neutrino flux is comparable to the 7.5 year averaged flux prediction from this source by IceCube.

The maximum proton energy for photohadronic interactions in the AGN frame is $E_{p,\text{max}} = \Gamma E'_{p,\text{max}} \approx 0.17 \text{ EeV}$. Assuming the protons escape efficiently beyond this energy and up to 100 EeV as UHECRs we calculate the cosmogenic γ -ray spectrum resulting from their propagation in the EGMF and interactions with the CMB and EBL photons. Secondaries from these interactions initiate electromagnetic cascade in the extragalactic medium, undergoing synchrotron radiation in the EGMF, pair production with EBL, inverse IC scattering of background photons, etc. The resulting spectrum is shown by the grey line in Fig. 1. Note that the cascade is sufficiently developed for $E_{p,\text{max}} \gtrsim 40 \text{ EeV}$, the GZK energy, then it depends more on the propagation effects than on the source parameters. The upcoming γ -ray telescope CTA will be detecting γ rays in the 20 GeV up to several hundred TeV range with unprecedented sensitivity. The orange dashed line in Fig. 1 shows the differential point source sensitivity of

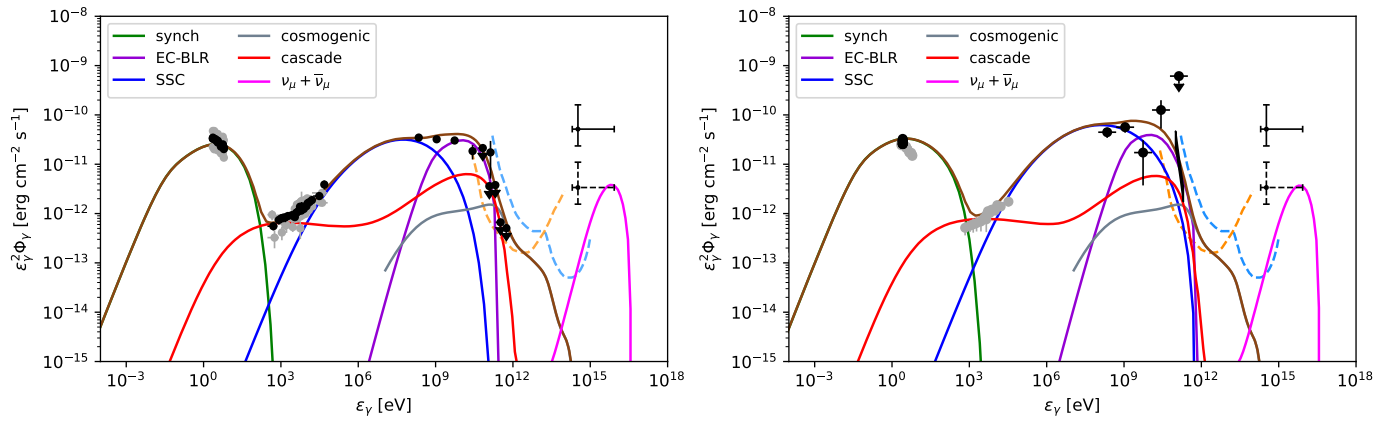


Fig. 1. Multiwavelength SED of TXS 0506+056 during the 2017-2019 campaign. *Left:* Low-state (average) flux during the observation period. Black data points show the Fermi-LAT average spectrum and MAGIC upper limits, and Swift and NuSTAR spectra on 2018 October 16. Gray data points show the whole range of optical-to-X-ray spectra. *Right:* High-state observation in VHE γ -rays during 2018 December. Black data points show the Fermi-LAT, MAGIC, and ASAS-SN contemporaneous spectra. Gray data points show the nearest observations in radio, optical, UV, and X-rays on 2018 December 8. The green, blue, and purple lines corresponds to SYN, SSC, and EC-BLR emission. The red line is the cascade emission from secondary electrons. The magenta line is the predicted neutrino flux in both cases. The grey line is the cosmogenic γ -ray flux from extragalactic propagation of UHE protons. The orange and blue dashed lines are CTA and LHAASO point source sensitivity. See text for details.

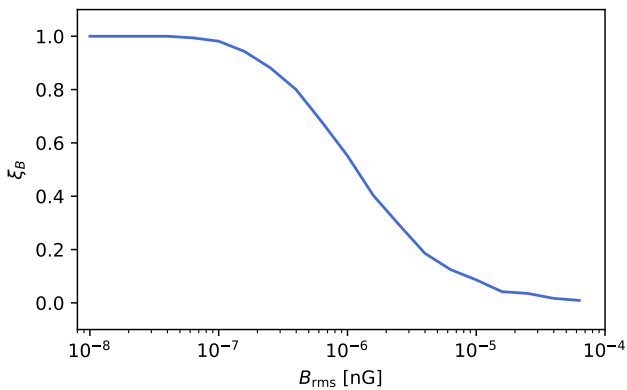


Fig. 2. Survival fraction of UHECRs along the line-of-sight, i.e., within 0.1° of the initial direction of propagation, as a function of the rms strength of EGMF.

CTA, assuming 50h observation time and pointing to 20 degrees zenith (Gueta 2021). It can be seen that CTA will be able to restrict our model if it detects multi-TeV γ -ray signal from this source. The blue dashed line is the LHAASO 1-yr sensitivity to Crab-like γ -ray point sources (Vernetto 2016).

We define the line-of-sight resolved component of the cosmogenic γ -ray spectrum as the fraction of UHECRs (ξ_B) that survive within 1° of the initial propagation direction, from the source to the observer, after deflection in the EGMF. For neutrinos of energy ~ 30 TeV, the angular resolution of IceCube for track-like events is $\sim 0.5^\circ$. Whereas, Fermi-LAT has a resolution of 3.5° to photons of energy < 100 MeV, and $\sim 0.15^\circ$ beyond 10 GeV. We use CRPropa-3 to propagate UHECRs in the extragalactic space (Alves Batista et al. 2016). ξ_B is calculated from arrival direction of protons in a 3D simulation on the surface of a sphere of radius 100 kpc, centered at the observer. We propagate a E^{-2} proton spectrum in the energy range between 0.1 and 100 EeV in a random turbulent magnetic field with a Kolmogorov power spectrum. The coherence length of the field is adjusted to 100 kpc. Thus, the secondary flux for a given luminosity is multiplied by ξ_B to obtain the line-of-sight component at the position of the observer (Das et al. 2020). The survival fraction ξ_B as a function of rms field strength is shown in Fig. 2.

The value of B_{rms} can be constrained from the required luminosity in cosmogenic γ -rays by the following expression, under isotropic approximation

$$\frac{L_{\text{UHE}p}}{4\pi d_L^2} = \frac{1}{\xi_B f_{\gamma,p}} \int_{\epsilon_{\gamma,\text{min}}}^{\epsilon_{\gamma,\text{max}}} \epsilon_{\gamma} \frac{dn}{d\epsilon_{\gamma} dAdt} d\epsilon_{\gamma} \quad (9)$$

where $dn/d\epsilon_{\gamma} dAdt$ is the differential flux of cosmogenic γ rays constrained by the SED. We calculate the electromagnetic cascade using the external code DINT integrated with CRPropa-3 (Heiter et al. 2018). The factor $f_{\gamma,p}$ takes into account the fraction of injected UHECR power that goes into cosmogenic γ rays, and is fairly constant with variation of B_{rms} . For TXS 0506+056 we find $f_{\gamma,p} \approx 0.156$. The integrated flux of cosmogenic photons along the line-of-sight of the observer, allowed by the observed SED is $\sim 1 \times 10^{-11}$ erg cm $^{-2}$ s $^{-1}$, as found from Fig. 1. The observed luminosity of protons interacting inside the jet is found to be $L_p^{\text{obs}} = 1.6 \times 10^{48}$ erg/s (cf. Tab. 1). Using the same normalization the observed luminosity in UHECR protons, i.e., between 0.1 – 100 EeV is $L_{\text{UHE}p} \approx 8 \times 10^{47}$ erg/s. This implies from Eq. (9), for the allowed flux of cosmogenic γ rays, $\xi_B \lesssim 0.05$. This indicates an EGMF with RMS value higher than few times 10^{-5} nG as seen from Fig. 2. There may be no cosmogenic component along the line-of-sight for magnetic field strength much larger than this, otherwise the luminosity budget is violated.

We calculate the flux of cosmogenic neutrinos produced simultaneously during the propagation of UHECRs, and use the same normalization as γ -ray spectrum. The cosmogenic neutrino spectrum peaks at 2.8×10^{18} eV with peak flux $\sim 4.5 \times 10^{-13}$ erg cm $^{-2}$ s $^{-1}$, shown in Fig. 3. The IceCube-Gen2 detector will be capable of detecting neutrinos from TeV to EeV energies, with sensitivity five times larger than currently operating IceCube experiment. We also show the 5σ sensitivity for detection of muon neutrino flux from TXS 0506+056, using the IceCube-Gen2 detector (Aartsen et al. 2021). The black and red lines correspond to 100 days and 10 years of observation and indicate the sensitivity for neutrino flares and the time-averaged neutrino emission, respectively. The neutrino flux is lower than the detection threshold, however. Thus the γ -rays provide more stringent limits on UHECR acceleration in TXS 0506+056.

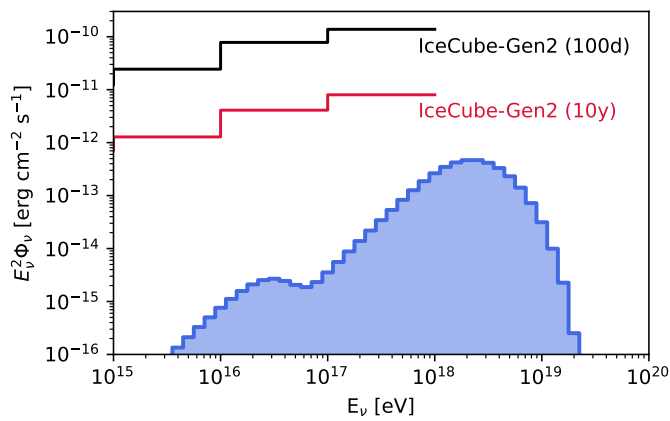


Fig. 3. All-flavor cosmogenic neutrino flux from TXS 0506+056 due to UHECR propagation along the line of sight, i.e., using the same normalization as the cosmogenic γ -ray spectrum in Fig. 1. The black and red curves correspond to 100 days and 10 years of observations of muon neutrino fluxes by IceCube-Gen2 and indicate the sensitivity for neutrino flares and the time-averaged neutrino emission, respectively.

3. Summary and Conclusions

The flux variability observed by MAGIC in December 2018 was very similar to that seen in 2017. No neutrino event was detected in 2018 however, in contrast to the 2017 flare, which is puzzling and implies that physical processes determining the γ -ray and neutrino flares are different. Emission from the pion-decay cascade is found to be sub-dominant in the GeV range but important in the X-ray and VHE bands. If the same physical process is responsible for the neutrino production, then the X-ray data constrain the neutrino flux to be consistent with IceCube prediction for one event in $\Delta T = 7.5$ yrs. Hence, an additional hidden sector must be invoked to explain the neutrino flare in 2017 and $\Delta T = 0.5$ yr flux. This is consistent with no observation of γ -ray activity during the orphan neutrino flare during 2014–15.

The lack of simultaneous X-ray data in the high-state is a drawback to the SED modeling, although the data points shown are that for the nearest observation on 2018 December 8. The parameters are varied minimally from the low-state to account for this. Interestingly, our modeling does not predict any significant flare of the optical flux, where the SYN spectrum peaks, but the UV and soft X-ray fluxes are expected to change moderately. We note that a higher X-ray flux can allow for an increased neutrino flux, however. But explaining the $\Delta T = 0.5$ yr neutrino flux remains difficult due to excess X-ray production.

The origin of external photons is a question of fundamental importance in the modeling of TXS-like blazars. In their modeling, MAGIC collaboration used an external field originating from the spine-layer or the jet-sheath (Ansoldi et al. 2018; Acciari et al. 2022). In our analysis, we consider it to originate from the BLR. It provides a substantial target for neutrino production by $p\gamma$ processes and also inverse-Compton scattering by electrons. For this to be true, the radius of the emission region must be smaller than the radius of the BLR region. The typical energy of the photons in the AGN frame is $\epsilon_{\text{ext}} \sim 3k_B T' / \Gamma \approx 17$ eV. This is comparable to that obtained in other studies (Keivani et al. 2018) and can also be considered as scattered emission from the disk. The contribution from disk photon itself is negligible.

Modeling the escape of UHECRs beyond a specific energy is difficult. A plausible alternative is to invoke a separate acceleration zone for protons with energy $E_p \gtrsim 0.1$ EeV. In our analysis, the cosmogenic γ -ray spectrum remains fixed for both the low-

and high-states. A change in the primary proton distribution will not affect the cosmogenic flux significantly, because the spectrum is driven greatly by parameters guiding the extragalactic propagation. Since UHECRs are delayed in the EGMF, any observed variability in the VHE regime occurs, most likely, due to an increased activity inside the jet. The required luminosity in UHE protons can also be translated into a resulting flux of neutrinos at EeV energies. The cosmogenic neutrino flux predicted here, from constraints on γ -ray flux, is found to be lower than that in our earlier study (Das et al. 2022). Thus detection of cosmogenic neutrinos from point sources seems unlikely with the next generation upgrade of IceCube, leaving ground-based γ -ray detectors such as CTA to test UHECR signature in the SED of blazars.

Acknowledgements. S.D. thanks Konstancja Satalecka (MAGIC Collaboration) for correspondence regarding the multiwavelength SED data. The work of S.D. was supported by JSPS KAKENHI Grant Number 20H05852. Numerical computation in this work was carried out at the Yukawa Institute Computer Facility.

References

- Aartsen, M. G. et al. 2018a, *Science*, 361, eaat1378
Aartsen, M. G. et al. 2018b, *Science*, 361, 147
Aartsen, M. G. et al. 2021, *J. Phys. G*, 48, 060501
Acciari, V. A. et al. 2022, *Astrophys. J.*, 927, 197
Alves Batista, R., Dundovic, A., Erdmann, M., et al. 2016, *JCAP*, 05, 038
Ansoldi, S. et al. 2018, *Astrophys. J. Lett.*, 863, L10
Banik, P. & Bhadra, A. 2019, *Phys. Rev. D*, 99, 103006
Boettcher, M., Reimer, A., Sweeney, K., & Prakash, A. 2013, *Astrophys. J.*, 768, 54
Cerruti, M., Zech, A., Boisson, C., et al. 2019, *Mon. Not. Roy. Astron. Soc.*, 483, L12, [Erratum: *Mon. Not. Roy. Astron. Soc.* 502, L21–L22 (2021)]
Das, S., Gupta, N., & Razaque, S. 2020, *Astrophys. J.*, 889, 149
Das, S., Gupta, N., & Razaque, S. 2021, *Astrophys. J.*, 910, 100
Das, S., Razaque, S., & Gupta, N. 2022, *Astron. Astrophys.*, 658, L6
Eichler, D. 1979, *Astrophys. J.*, 232, 106
Franckowiak, A. et al. 2020, *Astrophys. J.*, 893, 162
Garrappa, S. et al. 2019, *Astrophys. J.*, 880, 880:103
Gilmore, R. C., Somerville, R. S., Primack, J. R., & Domínguez, A. 2012, *Monthly Notices of the Royal Astronomical Society*, 422, 3189
Gould, R. J. & Schröder, G. P. 1967, *Phys. Rev.*, 155, 1404
Gueta, O. 2021, in *Proceedings of 37th International Cosmic Ray Conference — PoS(ICRC2021)*, Vol. 395, 885
Hahn, J. 2016, *PoS, ICRC2015*, 917
Heiter, C., Kuempel, D., Walz, D., & Erdmann, M. 2018, *Astroparticle Physics*, 102, 39
IceCube Collaboration, Aartsen, M., et al. 2013, *Science*, 342, 1242856
Kalashev, O. E., Kusenko, A., & Essey, W. 2013, *Phys. Rev. Lett.*, 111, 041103
Keivani, A. et al. 2018, *Astrophys. J.*, 864, 84
Kelner, S. R. & Aharonian, F. A. 2008, *Phys. Rev. D*, 78, 034013, [Erratum: *Phys. Rev. D* 82, 099901 (2010)]
Kochocki, A., Takhistov, V., Kusenko, A., & Whitehorn, N. 2021, *Astrophys. J.*, 914, 91
Liu, R.-Y., Wang, K., Xue, R., et al. 2019, *Phys. Rev. D*, 99, 063008
Padovani, P., Oikonomou, F., Petropoulou, M., Giommi, P., & Resconi, E. 2019, *Mon. Not. Roy. Astron. Soc.*, 484, L104
Petropoulou, M., Dimitrakoudis, S., Padovani, P., Mastichiadis, A., & Resconi, E. 2015, *Mon. Not. Roy. Astron. Soc.*, 448, 2412
Petropoulou, M. et al. 2020, *Astrophys. J.*, 891, 115
Reimer, A., Boettcher, M., & Buson, S. 2019, *Astrophys. J.*, 881, 46, [Erratum: *Astrophys. J.* 899, 168 (2020)]
Sahakyan, N. 2018, *Astrophys. J.*, 866, 109
Sikora, M., Kirk, J. G., Begelman, M. C., & Schneider, P. 1987, *Astrophys. J. Lett.*, 320, L81
Stecker, F. W. 1968, *Phys. Rev. Lett.*, 21, 1016
Vermetto, S. 2016, *J. Phys. Conf. Ser.*, 718, 052043
Xue, R., Liu, R.-Y., Wang, Z.-R., Ding, N., & Wang, X.-Y. 2021, *Astrophys. J.*, 906, 51
Yuan, C., Murase, K., & Mészáros, P. 2020, *ApJ*, 890, 25
Zhang, B. T., Petropoulou, M., Murase, K., & Oikonomou, F. 2020, *Astrophys. J.*, 889, 118